Electronic Supplementary Material (ESI) for Dalton Transactions.
This journal is © The Royal Society of Chemistry 2023

Supporting information

Efficient oxygen evolution reaction from iron-molybdenum nitride/molybdenum oxide heterostructured composites

Aijian Wang,*[a], Yuqin Dou[a], Xin Yang[a], Qi Wang[a], M. Shire Sudi[a], Long Zhao[a], Danhong Shang[b], Weihua Zhu[a], Jinshen Ren[a]

[a] School of Chemistry & Chemical Engineering, Jiangsu University, Zhenjiang 212013, P.R. China

[b] School of Energy & Power Engineering, Jiangsu University, Zhenjiang 212013, P.R. China

Corresponding Author. Tel: +86-511-88791928. E-mail: wajujs@ujs.edu.cn

Experimental section

Characterization

X-ray diffraction (XRD) pattern was recorded in a XD-3 diffractometer with Cu Kα radiation. Transmission electron microscopy (TEM) and scanning electron microscopy (SEM) of the samples were performed in a JEM-2100 HR, JEOL system), and a Model S4800, Hitachi, respectively. X-ray photoelectron spectroscopy (XPS) was conducted on a RBD upgraded PHI-5000C ESCA spectrometer.

Electrochemical measurements

All electrochemical measurements including oxygen evolution reaction were performed on a CHI 614E electrochemical workstation (CH Instrument, China) in 1.0 M KOH solution. The sample covered CFP is employed as the working electrode, a Pt gauze (1 × 1 cm^2) as the counter electrode and a mercury/mercury oxide electrode (MOE) as the reference electrode. The long-term stability of the samples was also examined by using the same electrolyzer. To prepare the working electrode, the catalysts (2 mg) and Nafion solution (5wt%, 40 μL) were dispersed in CH_3CH_2OH (0.5 mL), then the solution was sonicated for 1.0 h to give the homogeneous ink. Subsequently, the well-mixed suspension (100 μL) was loaded onto CFP. The obtained electrode was then dried naturally at room temperature and retained for use. The measured potential in this work has been calibrated with the reversible hydrogen electrode potential (RHE) based on Nernst equations. The measured LSV data were corrected by the following equation: $E_{compensated} = E_{measured}$ - iR (R represents the series resistance determined by EIS). The electrochemical impedance spectroscopy (EIS) measurement was recorded in the frequencies ranging from 0.01 Hz to 100 KHz with an amplitude of 1 mV. The double-layer capacitance of the as-synthesized samples is determined by the cyclic voltammograms with different scan rates (20, 40, 60, 80, and 100 mV/s) in the scope of 0.1-0.2 V *vs.* RHE. The oxygen quantification analysis was recorded in a gas chromatography instrument. The turnover frequencies (TOFs) per metal site are calculated based on the hypothesis that all the metal atoms in the catalysts formed active site and all of them were accessible to the electrolyte.[1] The following formula was applied to calculate the TOFs per active site in the as-prepared

samples:

TOFs = (#total oxygen turnover/cm^2 geometric area)/(#active sites/cm^2 geometric area); $\#O_2 = (J \times N_A)/(4F \times 1000)$

where the J represents the current density, N_A is the the Avogadro's number (6.02×10^{23}), and F is the Farada constant (96485 C mol^{-1}). The metal loading of the as-prepared samples is determined by the ICP measurements. It is noted that the number of practical active sites should be lower than the theoretical value.

Preparation of Mo_5N_6/MoO_3 catalyst

To prepare Mo_5N_6/MoO_3 composite, $(NH_4)_2MoO_4$ (1.23 g) and $C_2H_4N_4$ (0.1 g) were well dispersed in CH_3CH_2OH (20 mL) and deionized water (20 mL) by sonicating in an ultrasonic bath for 1 h. The mixture was transferred into 100 mL Teflon-lined stainless-steel autoclave that was heated at 160 ^oC for 12 h to afford the desired precursors. The obtained mixture was positioned in an alumina boat and heated at 550 ^oC for 3 h at a rate of 5 ^oC/min in a N_2 flow. After cooling down to room temperature, the final Mo_5N_6/MoO_3 composite was obtained by washing with ultrapure water and CH_3CH_2OH.

Preparation of Mo_5N_6 catalyst

The Mo_5N_6 catalyst was fabricated by annealing precursor $(NH_4)_2MoO_4$ (1.23 g) in pure ammonia atmosphere under the final conditions of 550 °C, 5 °C min^{-1}, and hold for 5 h. After cooling down to room temperature, the final Mo_5N_6 was obtained by washing with ultrapure water and CH_3CH_2OH.

Preparation of MoO_3 catalyst

To prepare MoO_3 electrocatalyst, $(NH_4)_2MoO_4$ (1.23 g) was well dispersed in CH_3CH_2OH (20 mL) and deionized water (20 mL) by sonicating in an ultrasonic bath for 1 h. The mixture was transferred into 100 mL Teflon-lined stainless-steel autoclave that was heated at 160 ^oC for 12 h to afford the desired precursors. The obtained mixture was positioned in an alumina boat and heated at 550 ^oC for 3 h at a rate of 5 ^oC/min in a N_2 flow. After cooling down to room temperature, the final MoO_3 was obtained by washing with ultrapure water and CH_3CH_2OH.

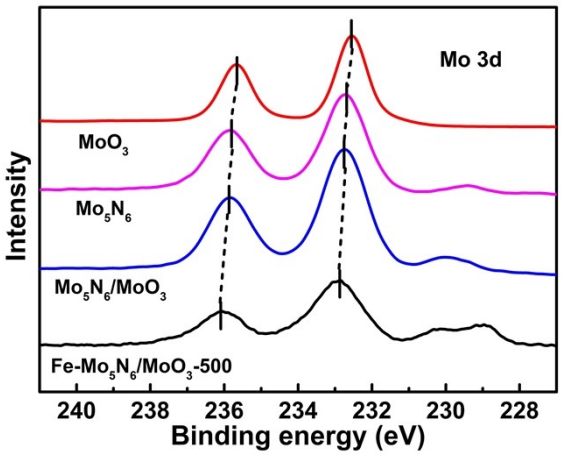

Figure S1. High resolution XPS spectra of Mo 3d for the as-prepared samples.

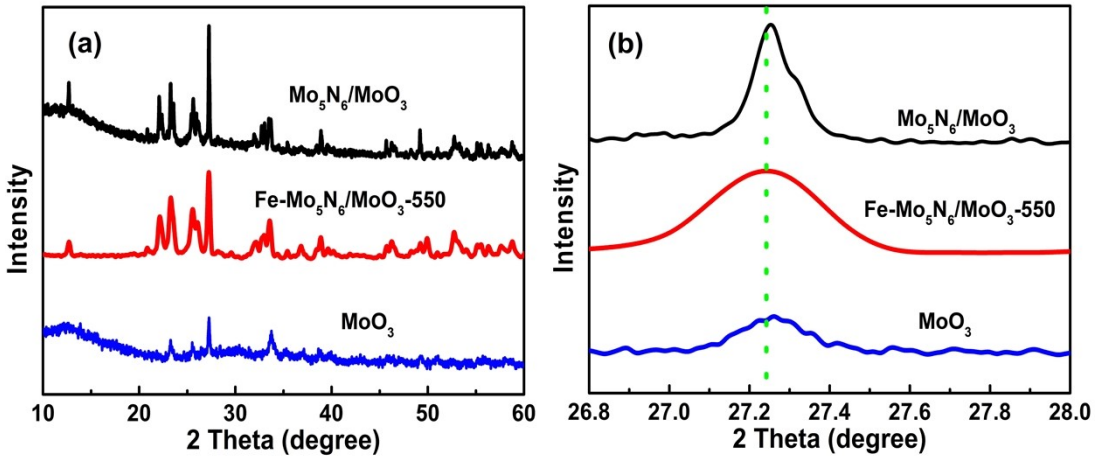

Figure S2. (a) XRD patterns and the enlarged image in the region of 26.8°-28.0° for the as-prepared samples.

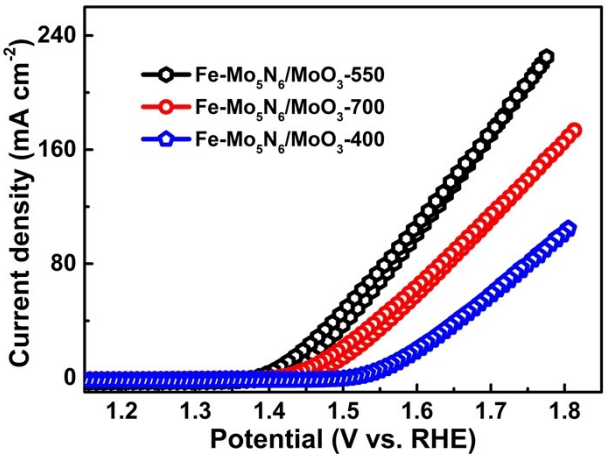

Figure S3. CV polarization curves of the as-prepared samples.

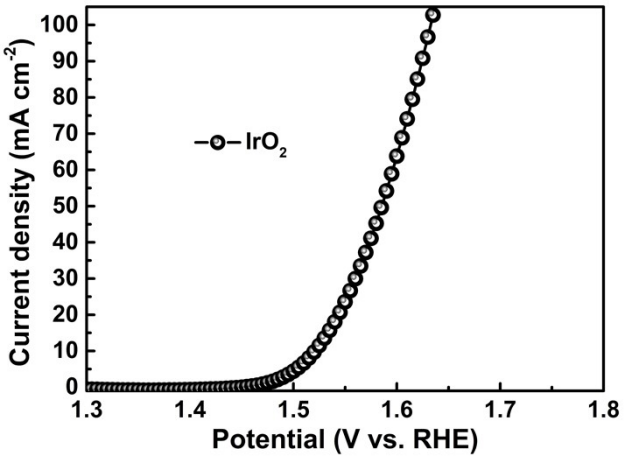

Figure S4. OER polarization curve of commercial IrO_2.

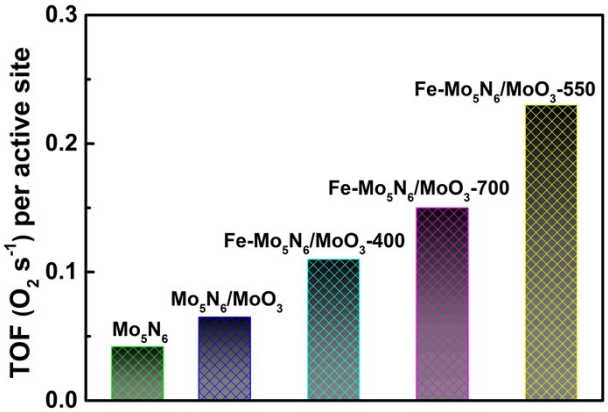

Figure S5. TOF values of the as-prepared samples for OER.

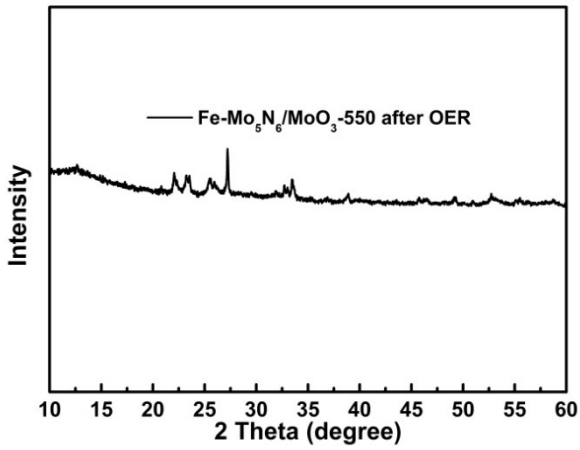

Figure S6. XRD pattern of Fe-Mo_5N_6/MoO_3-550 after OER.

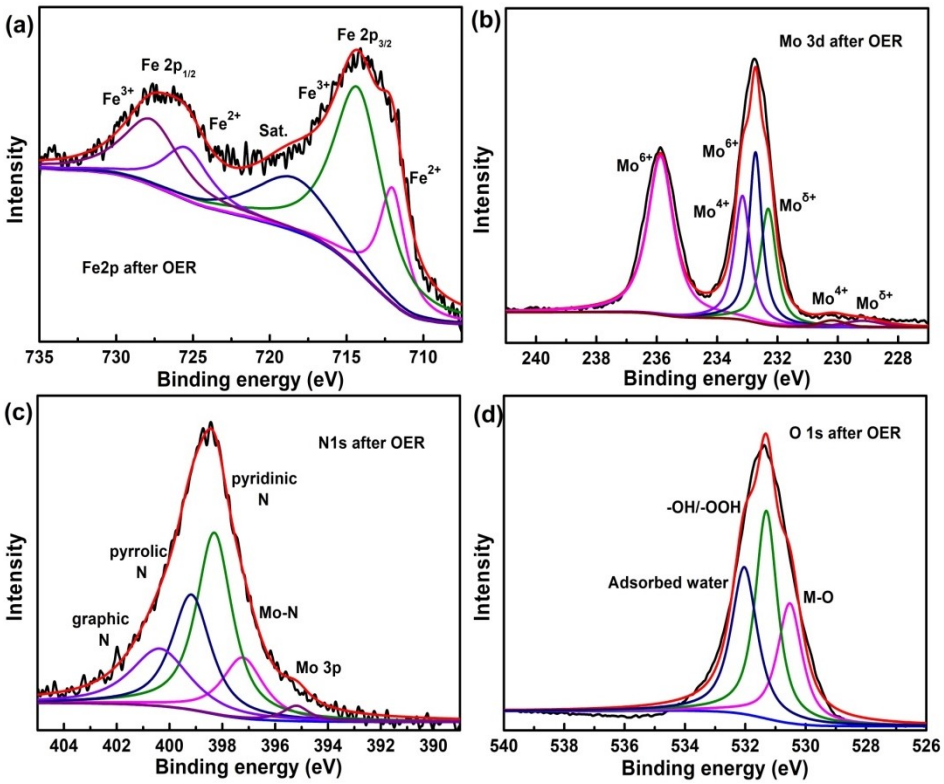

Figure S7. High resolution XPS spectra of (a) Fe 2p, (b) Mo 3d, (c) N 1s and (d) O 1s for Fe-Mo_5N_6/MoO_3-550 after OER.

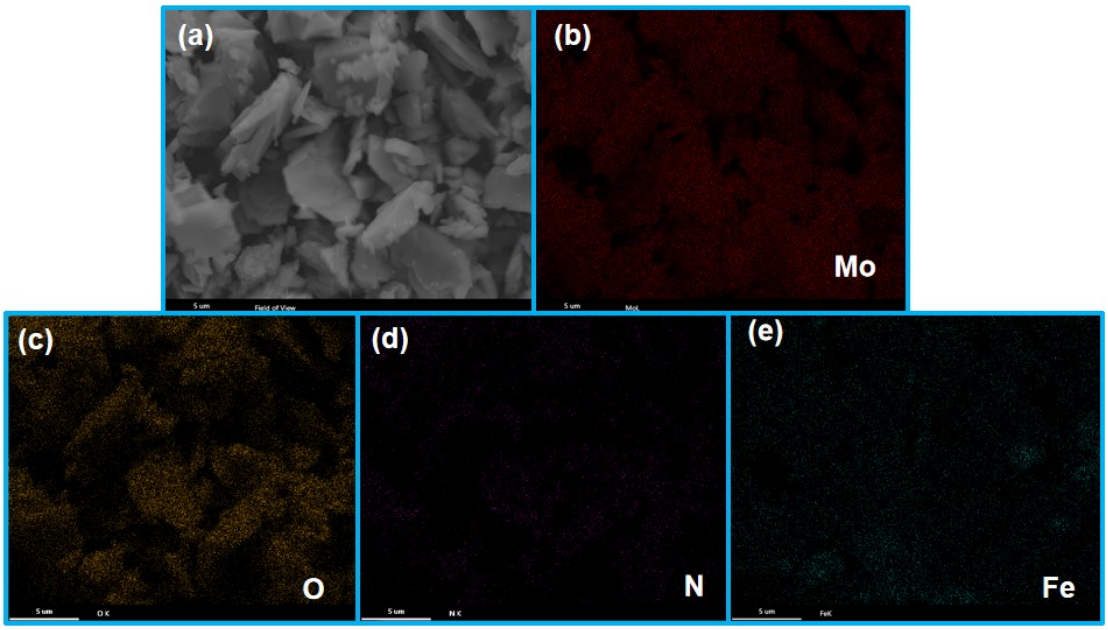

Figure S8. (a) SEM image, and the corresponding elemental mapping images of (b) Mo, (c) O, (d) N and (e) Fe for Fe-Mo_5N_6/MoO_3-550 after OER.

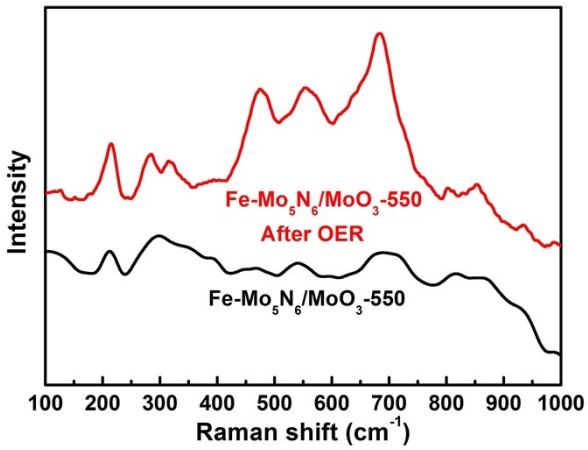

Figure S9. Raman spectra of Fe-Mo_5N_6/MoO_3-550 before and after OER.

For Fe-Mo_5N_6/MoO_3-550, some new peaks appeared after OER, which can be ascribed to the typical Raman vibrational peaks of the generated Fe oxides/oxy(hydroxides) during OER process.[1-5]

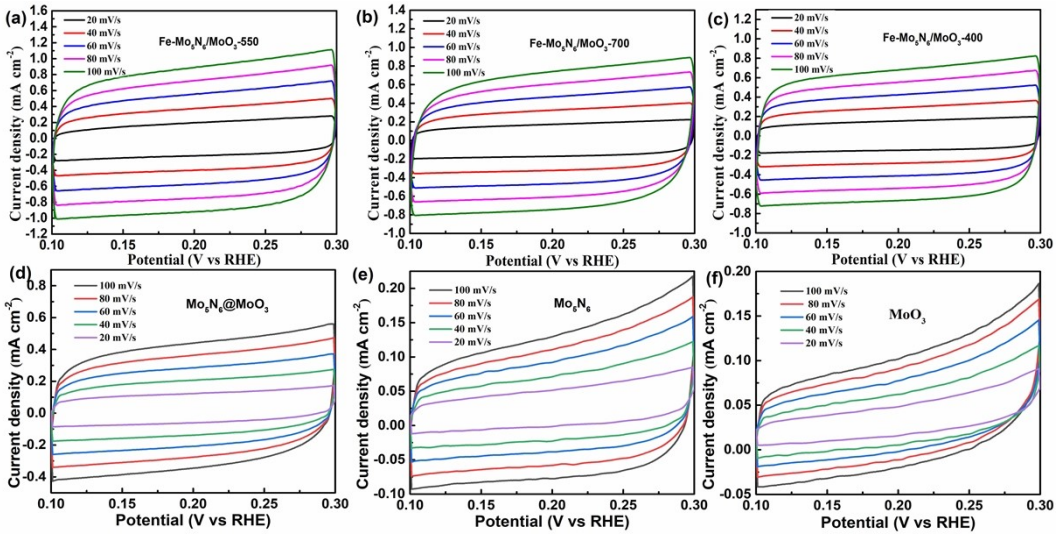

Figure S10. CV curves of the samples at different scan rates.

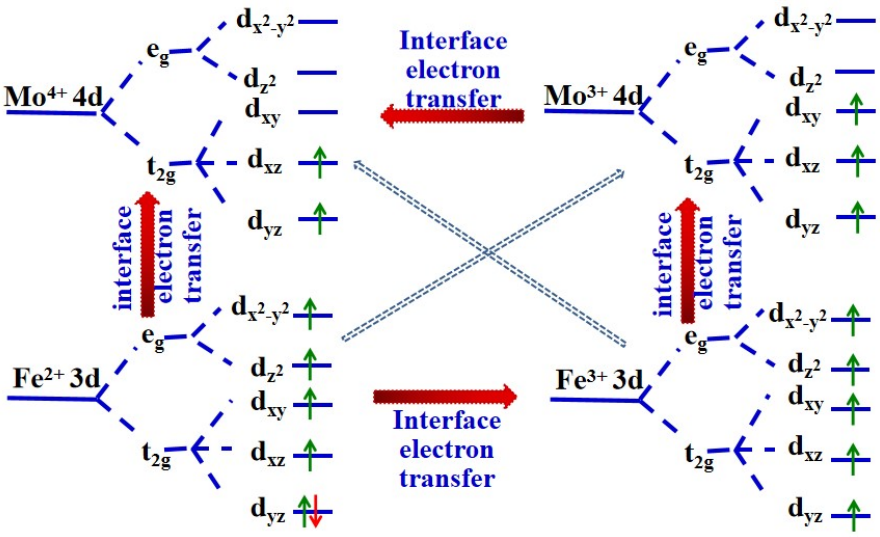

Figure S11. Systematic representation of electronic configuration in the case of Fe^{2+}, Fe^{3+}, Mo^{3+} and Mo^{4+} and possible electron transfer. Mo^{6+} is not presented in this case. The partial electron transfer from the electron-rich t_{2g} d-orbitals (Fe^{2+}, Fe^{3+}, Mo^{3+} and Mo^{4+}) to the electron-deficient t_{2g} d-orbitals (Mo^{6+}) can be occurred through the bridging O^{2-} at the interface, since the π-symmetry t_{2g} d-orbitals of Mo^{6+} are fully unoccupied.

Table S1. Comparison of catalytic activity for OER on different catalysts.

Catalyst	Overpotential at 10 mA·cm^{-2} (η_{10}, mV vs. RHE)	Overpotential at 100 mA·cm^{-2} (η_{100}, mV vs. RHE)	Reference
MoO_3/Ni–NiO	/	347	1
$LaFe_xNi_{1-x}O_3$	302	/	6
NiO@MoO_3/VC	280	/	7
Fe_2Ni-BPTC	365	/	8
NiFe LDH	300	/	9
P-MoO_3 FCL MXene/NF	179	/	10
S-$NiFe_2O_4$/NF	267	/	11
Ti_3C_2@MoO_3	190	/	12
$NiFe_2O_4$	381	/	13
ZIF67@MoO_3 NSs@NF	178	/	14
$Ni_{0.65}Fe_{0.35}P$	270	/	15
Fe-doped MoO_2/MoO_3	/	310	16
NiFeLDH/CNT	308	/	17
$Ni(PO_3)_2$–MoO_3/NF	234	/	18
Co_3O_4/MoO_3/g-C_3N_4	206	/	19
NiO@MoO_3/VC	280	/	20
Mo-doped Ni_3Fe/Ni_3FeN	240	/	21
Co-Mo-N@Ag	234	346	22
Co-NiMoN-400 NRs	294	367	23
Ni/MoN@NCNT/CC	252	368	24
Ni_3FeN	223	/	25
$CuMo_2ON$@NG	180	/	26
Ni_3N-NiMoN	227	> 340	27
NiMoN	202	> 350	28
Mo–N-CNT	344	/	29
Ni/$Ni_{0.2}Mo_{0.8}N$/MoO_3	252	> 370	30
CoMoNx-500 NSAs/NF	231	> 315	31
Co/Ce-Ni_3S_2/NF	286 (η_{20})	> 370	32
Fe, O–Ni_2P	210	/	33
NiFe-codoped PCN	270	/	34
Fe-doped Ni_3Se_4	225	/	35
Fe doped $NiSe_2$	227	/	36
NiFe−$W_{18}O_{49}$	325	/	37
Mo-doped CoP_2	220	306	38
Ni_3S_2/MoS_2/20g-C_3N_4	183	/	39
FeO_x-MoP@MWCNTs-2	229	> 330	40
CoSe@$NiSe_2$@MoS_2	170	> 370	41
Fe-Mo_5N_6/MoO_3-550	**201**	**373**	**This work**
Fe-Mo_5N_6/MoO_3-550	**216 (η_{20})**	**373**	**This work**

References

1. X. Li, Y. Wang, J. Wang, Y. Da, J. Zhang, L. Li, C. Zhong, Y. Deng, X. Han, W. Hu, Sequential Electrodeposition of Bifunctional Catalytically Active Structures in MoO_3/Ni–NiO Composite Electrocatalysts for Selective Hydrogen and Oxygen Evolution, Adv. Mater. 2020, 32, 2003414.
2. C. T. Moi, S. Bhowmick, M. Qureshi, Hierarchical FeO(OH)−CoCeV (Oxy)hydroxide as a Water Cleavage Promoter, ACS Appl. Mater. Interfaces 2021, 13, 51151−51160.
3. H. Tang, L. Lv, H. Xian, L. Ran, B. Chen, Y. Fu, Y. Wu, M. Fan, H. Wan, H. Wang, Interfacial electronic coupling in Mn_3O_4/C@FeOOH nano-octahedrals regulates intermediate adsorption for highly efficient oxygen evolution reaction, Appl. Surf. Sci., 2023, 612, 155951.
4. S. Chandrasekaran, E. J. Kim, J. S. Chung, C. R. Bowen, B. Rajagopalan, V. Adamaki, R. D. K. Misrac, S. H. Hur, High performance bifunctional electrocatalytic activity of a reduced graphene oxide–molybdenum oxide hybrid catalyst, J. Mater. Chem. A, 2016, 4, 13271-13279.
5. C. Pi, X. Li, X. Zhang, H. Song, Y. Zheng, B. Gao, A. Kızılaslan, P. K. Chu, K. Huo, In-Plane Mott–Schottky Effects Enabling Efficient Hydrogen Evolution from Mo_5N_6-MoS_2 Heterojunction Nanosheets in Universal-pH Electrolytes, Small, 2022, 18, 2201137.
6. H. Wang, J. Wang, Y. Pi, Q. Shao, Y. Tan, X. Huang, Double Perovskite $LaFe_xNi_{1-x}O_3$ Nanorods Enable Efficient Oxygen Evolution Electrocatalysis. Angew. Chem. Int. Ed. 2019, 58, 2316-2320.
7. R. Illathvalappil, L. George, S. Kurungot, Coexisting Few-Layer Assemblies of NiO and MoO_3 Deposited on Vulcan Carbon as an Effiffifficient and Durable Electrocatalyst for Water Oxidation, ACS Appl. Energy Mater. 2019, 2, 4987−4998.
8. X. L. Wang, L. Z. Dong, M. Qiao, Y. J. Tang, J. Liu, Y. Li, S. L. Li, J. X. Su, Y. Q. Lan, Exploring the Performance Improvement of Oxygen Evolution Reaction in Stable Bimetal -Organic Framework System. Angew. Chem. Int. Ed. 2018, 57, 9660-9664.
9. F. Song and X. Hu, Exfoliation of Layered Double Hydroxides for Enhanced Oxygen Evolution Catalysis. Nat. Commun. 2014, 5, 4477.
10. M. Li, R. Sun, Y. Li, J. Jiang, W. Xu, H. Cong, S. Han, The 3D porous “celosia”

heterogeneous interface engineering of layered double hydroxide and P-doped molybdenum oxide on MXene promotes overall water-splitting, Chem. Eng. J. 2022, 431, 133941.

11. J. Liu, D. Zhu, T. Ling, A. Vasileff, S. Z. Qiao, S-$NiFe_2O_4$ Ultra-small Nanoparticle Built Nanosheets for Efficient Water Splitting in Alkaline and Neutral pH. Nano Energy 2017, 40, 264-273.
12. I. Ashraf, S. Ahmad, S. Rizwan, M. Iqbal, Fabrication of Ti_3C_2@MoO_3 nanocomposite as an electrode material for highly efficient and durable water splitting system, Fuel, 2021, 299, 120928.
13. V. Maruthapandian, M. Mathankumar, V. Saraswathy, B. Subramanian, S. Muralidharan, A Study of Oxygen Evolution Reaction Catalytic Behavior of $Co_xNi_{1-x}Fe_2O_4$ in Alkaline Medium. ACS Appl. Mater. Interfaces. 9 (2017) 13132-3141.
14. X. Wei, Y. Chai, N. Liu, S. Qiao, Y. Fu, S. Chong, ZIF67@MoO_3 NSs@NF composite electrocatalysts reinforced by chemical bonds and oxygen vacancy for effificient oxygen evolution reaction and overall water-splitting, Int. J. Hydrogen Energy, 2022, 47, 9606-9615.
15. Z. Liu, G. Zhang, K. Zhang, H. Liu, J. Qu, Facile Dispersion of Nanosized NiFeP for Highly Effective Catalysis of Oxygen Evolution Reaction. ACS Sustainable Chem. Eng. 2018, 6, 7206-7211.
16. J. Chen, Q. Zeng, X. Qi, B. Peng, L. Xu, C. Liu, T. Liang, High-performance bifunctional Fe-doped molybdenum oxide-based electrocatalysts with in situ grown epitaxial heterojunctions for overall water splitting, Int. J. Hydrogen Energy, 2020, 45, 24828-24839.
17. M. Gong, Y. Li, H. Wang, Y. Liang, J. Z. Wu, J. Zhou, J. Wang, T. Regier, F. Wei, H. Dai, An Advanced Ni–Fe Layered Double Hydroxide Electrocatalyst for Water Oxidation. J. Am. Chem. Soc. 135 (2013) 8452-8455.
18. K. Li, J. Ma, X. Guan, H. He, M. Wang, G. Zhang, F. Zhang, X. Fan, W. Peng, Y. Li, 3D self-supported $Ni(PO_3)_2$–MoO_3 nanorods anchored on nickel foam for highly effiffifficient overall water splitting, Nanoscale, 2018, 10, 22173–22179.
19. I. Ahmed, R. Biswas, R. A. Patil, K. K. Halder, H. Singh, B. Banerjee, B. Kumar, Y. Ma,

K. K. Haldar, Graphitic Carbon Nitride Composites with MoO3-Decorated Co3O4 Nanorods as Catalysts for Oxygen and Hydrogen Evolution, ACS Appl. Nano Mater. 2021, 4, 12672−12681.

20. R. Illathvalappil, L. George, S. Kurungot,Coexisting Few-Layer Assemblies of NiO and MoO_3 Deposited on Vulcan Carbon as an Efficient and Durable Electrocatalyst for Water Oxidation, ACS Appl. Energy Mater. 2019, 2, 4987−4998.
21. Z. Shao, J. Sun, Z. Yan, K. Huang, F. Tian, H. Xue, Q. Wang, Dual-modulation of phase and electronic structure in hierarchical Ni3Fe/Ni3FeN catalyst by Mo-doping to achieve effiffifficient oxygen evolution reaction, Appl. Surf. Sci. 2020, 529, 147172.
22. F. Jiao, J. Wang, Y. Lin, J. Li, X. Jing, Y. Gong, Sliver nanoparticles decorated Co-Mo nitride for efficient water splitting, Appl. Surf. Sci. 2021, 553, 149440.
23. Z. Yin, Y. Sun, Y. Jiang, F. Yan, C. Zhu, Y. Chen, Hierarchical Cobalt-Doped Molybdenum−Nickel Nitride Nanowires as Multifunctional Electrocatalysts, ACS Appl. Mater. Interfaces 2019, 11, 27751−27759
24. P. Wang, J. Qi, C. Li, X. Chen, T. Wang, C. Liang, N-doped Carbon Nanotubes Encapsulating Ni/MoN Heterostructures Grown on Carbon Cloth for Overall Water Splitting, ChemElectroChem 2020, 7, 745-752.
25. Y. Wang, C. Xie, D. Liu, X. Huang, J. Huo, S. Wang,Nanoparticle-Stacked Porous Nickel−Iron Nitride Nanosheet: A Highly Efficient Bifunctional Electrocatalyst for Overall Water Splitting, ACS Appl. Mater. Interfaces 2016, 8, 18652−18657.
26. J. Balamurugan, T. T. Nguyen, N. H. Kim, D. H. Kim, J. H. Lee, Novel core-shell CuMo-oxynitride@N-doped graphene nanohybrid as multifunctional catalysts for rechargeable zinc-air batteries and water splitting, Nano Energy, 2021, 85, 105987.
27. A. Wu, Y. Xie, H. Ma, C. Tian, Y. Gu, H. Yan, X. Zhang, G. Yang, H. Fu, Integrating the active OER and HER components as the heterostructures for the efficient overall water splitting, Nano Energy, 2018, 44, 353–363.
28. Y. Zhang, B. Zhang, Z. Yin, X. Ma, Y. Zhou, Bimetallic Ni–Mo nitride@N-doped C as highly active and stable bifunctional electrocatalysts for full water splitting, New J. Chem., 2022,46, 11893-11901.
29. S. Ji, W. Chen, Z. Zhao, X. Yu, H. S. Park, Molybdenum oxynitride nanoparticles on

nitrogen doped CNT architectures for the oxygen evolution reaction, Nanoscale Adv., 2020,2, 5659-5665.

30. R. Li, S. Li, M. Lu, Y. Shi , K. Qu, Y. Zhu, Energy-effificient hydrogen production over a high-performance bifunctional NiMo-based nanorods electrode, J. Colloid Interf. Sci., 2020, 571, 48–54.
31. Y. Lu, Z. Li, Y. Xu , L. Tang , S. Xu, D. Li , J. Zhu, D. Jiang, Bimetallic Co-Mo nitride nanosheet arrays as high-performance bifunctional electrocatalysts for overall water splitting, Chem. Eng. J. 2021, 411, 128433.
32. X. Wu, T. Zhang, Ji. Wei, P. Feng, X. Yan, Y. Tang, Facile synthesis of Co and Ce dual-doped Ni_3S_2 nanosheets on Ni foam for enhanced oxygen evolution reaction, Nano Res. 2020, 13(8), 2130–2135.
33. B. Xua, X. Yang, Q. Fang, L. Dua, Y. Fu, Y. Sun, Q. Liu, Q. Lin, C. Li,Anion-cation dual doping: An effective electronic modulation strategy of Ni_2P for high-performance oxygen evolution, J. Energy Chem., 2020, 48, 116–121.
34. C. Wu, X. Zhang, Z. Xia, M. Shu, H. Li, X. Xu, R. Si, A. I. Rykov, J Wang, S. Yu, S. Wang, G. Sun, Insight into the role of Ni–Fe dual sites in the oxygen evolution reaction based on atomically metal-doped polymeric carbon nitride, J. Mater. Chem. A, 2019, 7, 14001–14010.
35. J. Du, Z. Zou, C. Liu, C. Xu,Hierarchical Fe-doped Ni_3Se_4 ultrathin nanosheets as an effiffifficient electrocatalyst for oxygen evolution reaction, Nanoscale, 2018, 10, 5163–5170.
36. Y. Du, G. Cheng, W. Luo, Colloidal synthesis of urchin-like Fe doped $NiSe_2$ for efficient oxygen evolution, Nanoscale, 2017, 9, 6821–6825.
37. W. Hu, M. Tian, K. Zeng, J. Yan, J. Zhou, J. Zhang, M. H. Rummeli, H. Wang, R. Yang, Tuning the Electronic Structure of $W_{18}O_{49}$ via Dual Doping for Efficient Oxygen Evolution Reaction, ACS Appl. Energy Mater. 2022, 5, 3208−3216.
38. A. Wang, X. Chen, L. Cheng, X. Shen, W. Zhu, L. Li, J. Pang, Insights into the synergistic effffect of multi-walled carbon nanotube decorated Mo-doped CoP_2 hybrid electrocatalysts toward effiffifficient and durable overall water splitting, J. Mater. Chem. A, 2020, 8, 17621–17633.

39. H. Wang, J. Ren, A. Wang, Q. Wang, W. Zhao, L. Zhao, Synergistic catalysis of graphitic carbon nitride supported bimetallic sulfide nanostructures for efficient oxygen generation, Chem. Commun., 2022, 58, 9202–9205.
40. A. Wang, X. Shen, Y. Wang, Q. Wang, L. Cheng, X. Chen, C. Lv, W. Zhu, L. Li, Rational design of FeOx-MoP@MWCNT composite electrocatalysts toward effifffifficient overall water Splitting, Chem. Commun., 2021, 57, 6149–6152.
41. X. Shen, M. Zhang, M. S. Sudi, W. Zhao, Q. Wang, J. Ren, L. Zhao, A. Wang, W. Zhu, Synergistic optimization promoted overall water splitting of CoSe@$NiSe_2$@MoS_2 heterostructured composites, Chem. Commun., 2021,57, 12516-12519.